

Microstructural Features Controlling Mechanical Properties in Nb-Mo Microalloyed Steels. Part II: Impact Toughness

NEREA ISASTI, DENIS JORGE-BADIOLA, MITRA L. TAHERI, and PELLO URANGA

The present paper is the final part of a two-part paper where the influence of coiling temperature on the final microstructure and mechanical properties of Nb-Mo microalloyed steels is described. More specifically, this second paper deals with the different mechanisms affecting impact toughness. A detailed microstructural characterization and the relations linking the microstructural parameters and the tensile properties have already been discussed in Part I. Using these results as a starting point, the present work takes a step forward and develops a methodology for consistently incorporating the effect of the microstructural heterogeneity into the existing relations that link the Charpy impact toughness to the microstructure. In conventional heat treatments or rolling schedules, the microstructure can be properly described by its mean attributes, and the ductile–brittle transition temperatures measured by Charpy tests can be properly predicted. However, when different microalloying elements are added and multiphase microstructures are formed, the influences of microstructural heterogeneity and secondary hard phases have to be included in a modified equation in order to accurately predict the DB transition temperature in Nb and Nb-Mo microalloyed steels.

DOI: 10.1007/s11661-014-2451-6

© The Minerals, Metals & Materials Society and ASM International 2014

I. INTRODUCTION

THE current demand for ultrahigh strength steels with high toughness at low temperatures covers different structural applications, such as the oil and gas industry and heavy equipment for naval, construction, and automotive applications.^[1,2] Traditional thermomechanical-controlled processing (TMCP) of microalloyed steels is employed to refine the microstructure and produce multi-phase microstructures, which provides good combinations of high strength and low temperature impact toughness. Suitable processing parameters in conjunction with microalloying help improve strength through various mechanisms: microstructural refinement, solid solution hardening, precipitation strengthening, and dislocation hardening due to the modification of the resulting microstructure.^[3] However, although strength levels can be increased by different combinations of the strengthening mechanisms, toughness properties may be impaired. Grain size refinement is the only mechanism that increases yield strength and reduces the impact transition temperature. Therefore, a careful design of chemical combination and process parameters is needed in order to meet strength and toughness properties simultaneously.^[2,4]

The correlation between toughness properties and the different microstructural aspects is an issue that has not yet been solved. Significant efforts have been dedicated to investigating fracture toughness in different microstructures.^[5] Furthermore, when the final microstructure contains non-polygonal bainitic phases, the analysis of fracture toughness becomes more complex, due to the limitations related to the optical microscopy capacity.^[6] The electron-backscattered diffraction (EBSD) technique allows the mentioned limitations to be overcome and opens a broad range of possibilities in terms of microstructural characterization, which helps provide a better understanding of the influence of the microstructural parameters in the obtained mechanical properties.^[7,8] For example, grain boundary misorientation is essential as boundary nature controls different mechanical properties. Medium angle boundaries are considered to control strength properties by blocking dislocation movement, whereas high angle boundaries act as effective barriers to cleavage fracture.^[9] Therefore, the relations that link the microstructural parameters and transition temperatures can be expanded from ferrite–pearlite microstructures^[10] to more complex microstructures^[11] using EBSD.

Most of the semi-empirical equations reported in the literature for predicting ductile brittle transition temperatures (DBTT) were fitted to homogeneous microstructures.^[9] In those situations, the mean unit size value was a proper parameter for characterizing the whole ferrite microstructure. However, in microstructures obtained directly from hot rolling and/or with complex phases this condition is not always fulfilled. In these situations, the mean unit size will not properly describe the effect of this parameter on the DBTT empirical equations and therefore the inclusion of some parameter

NEREA ISASTI and DENIS JORGE-BADIOLA, Researchers, and PELLO URANGA, Researcher and Associate Professor, are with the CEIT and TECNUN (University of Navarra), Paseo de Manuel Lardizabal 15, 20018, Donostia-San Sebastián, Basque Country, Spain. Contact e-mail: puranga@ceit.es MITRA L. TAHERI, Hoeganaes Assistant Professor, is with the Department of Materials Science, Drexel University, Lebow 344, 3141 Chestnut Street, Philadelphia, PA 19104.

Manuscript submitted February 12, 2014.

Article published online July 16, 2014

that takes into account microstructural heterogeneity is needed. In addition to this and due to the weakest link character of the brittle fracture process, the volume fraction of the coarsest units becomes more relevant than the mean unit size. Some proposals have been put forth in order to take this effect into account. For example, Bingley considers the average size of the largest 20 pct of the grains in the distribution instead of the mean grain size value.^[12]

The present work is largely focused on the study of impact toughness properties and concentrates on providing a better understanding of the link between transition temperatures and microstructural features. Plane compression tests were carried out by varying the final coiling temperature in order to generate different microstructures. The relations between the microstructural aspects and tensile properties were already discussed in Part I.^[3] In this second part, the influences of microstructural heterogeneity and secondary hard phases are included in a modified equation to predict the ductile–brittle transition temperature (DBTT).

II. EXPERIMENTAL PROCEDURE

The compositions of the steels studied are shown in Table I. Plane strain compression tests were performed in order to generate different microstructures and to evaluate the effect of the coiling temperature and the composition on the final impact toughness properties.

The samples were reheated at 1523 K (1250 °C) for 5 minutes and quenched, in order to insure the dissolution of Nb precipitates, followed by a soaking at 1323 K (1050 °C) for 5 minutes. Afterward, the specimens were deformed in the plane compression machine in the non-recrystallization temperature region [1173 K (900 °C)], applying a strain of 0.4 at 1 s⁻¹. After a holding time of 5 seconds, the samples were cooled down at a constant rate of 10 K/s to three different coiling temperatures: 723 K, 823 K, and 923 K (450 °C, 550 °C, and 650 °C). Coiling was simulated by holding the samples for 1 hour followed by slow cooling in the furnace to room temperature at 1 K/s. More details regarding experimental setup can be found in Reference 3.

Charpy tests were performed in a Tinius Olsen Model Impact 104 pendulum impact tester with maximum capacity of 410 J. The Charpy samples were machined from the central area of the plane strain compression samples and due to geometrical constraints, subsize specimens (10 × 8 × 55 mm³) were obtained. Specimens

with a thickness of 8 mm are within the range of applicability of the proportionality rule^[13]:

$$K_{v_{10}} = \frac{10}{B} K_{v_B}, \quad [1]$$

where $K_{v_{10}}$ and K_{v_B} are the impact energy for specimens that are 10 mm or B mm thick, respectively.

The specimens used for the microstructural characterization were also obtained from the central part of the plane strain specimens. The microstructures were characterized after etching in 2 pct Nital by different characterization techniques: Optical Microscopy (OM, Olympus IX2-UCB), Scanning Electron Microscopy (SEM, Philips XL30CP), and Field-Emission Gun Scanning Electron Microscopy (FEGSEM, JEOL JSM-7000 F). Martensite–austenite (MA) island volume fractions as well as MA mean sizes (D_{MA}) were determined by quantitative metallography^[14] on optical micrographs, after a preparation using standard metallographic techniques and final etching in LePera reagent.^[15]

EBSD scans were performed, in order to obtain crystallographic features. The samples were polished down to 1 μm and the final polishing was performed with colloidal silica. These scans were done on the Philips XL30CP SEM with W-filament, using TSL (TexSEM Laboratories, UT) equipment. Different scan step sizes were defined depending on the resolution needed, varying from 0.1 μm for high resolution scans to 0.2 μm for general microstructural characterization and unit size measurements. The total scanned area was about 35 × 35 μm² and 400 × 400 μm², for the 0.1 and 0.2 μm step sizes, respectively.

III. RESULTS

In Figure 1, the absorbed energy is plotted as a function of test temperature for steels 3NbMo0, 3NbMo31, 6NbMo0, and 6NbMo31. Impact transition curves were determined with the modified hyperbolic tangent fitting algorithm by Wallin.^[16] Table II summarizes the transition temperatures for an impact energy value of 27 J (ITT 27 J) and for the temperature at which the sample shows a 50 pct ductile–brittle appearance (DBTT), as well as upper-shelf energy values for ductile fracture (US) calculated from the curves in Figure 1. As a general trend, it can be noticed that a decrease in coiling temperature shifts the impact transition curve to lower temperatures. Therefore as coiling temperature decreases, better toughness behavior is achieved. In reference to the effect of the composition

Table I. Chemical Composition of the Steels (in Weight Percent)

Steel	C	Mn	Si	Nb	Mo	Al	N
3NbMo0	0.05	1.6	0.06	0.029	0.01	0.028	0.005
3NbMo31	0.05	1.57	0.05	0.028	0.31	0.028	0.005
6NbMo0	0.05	1.56	0.05	0.06	0.01	0.028	0.004
6NbMo31	0.05	1.57	0.05	0.059	0.31	0.031	0.005

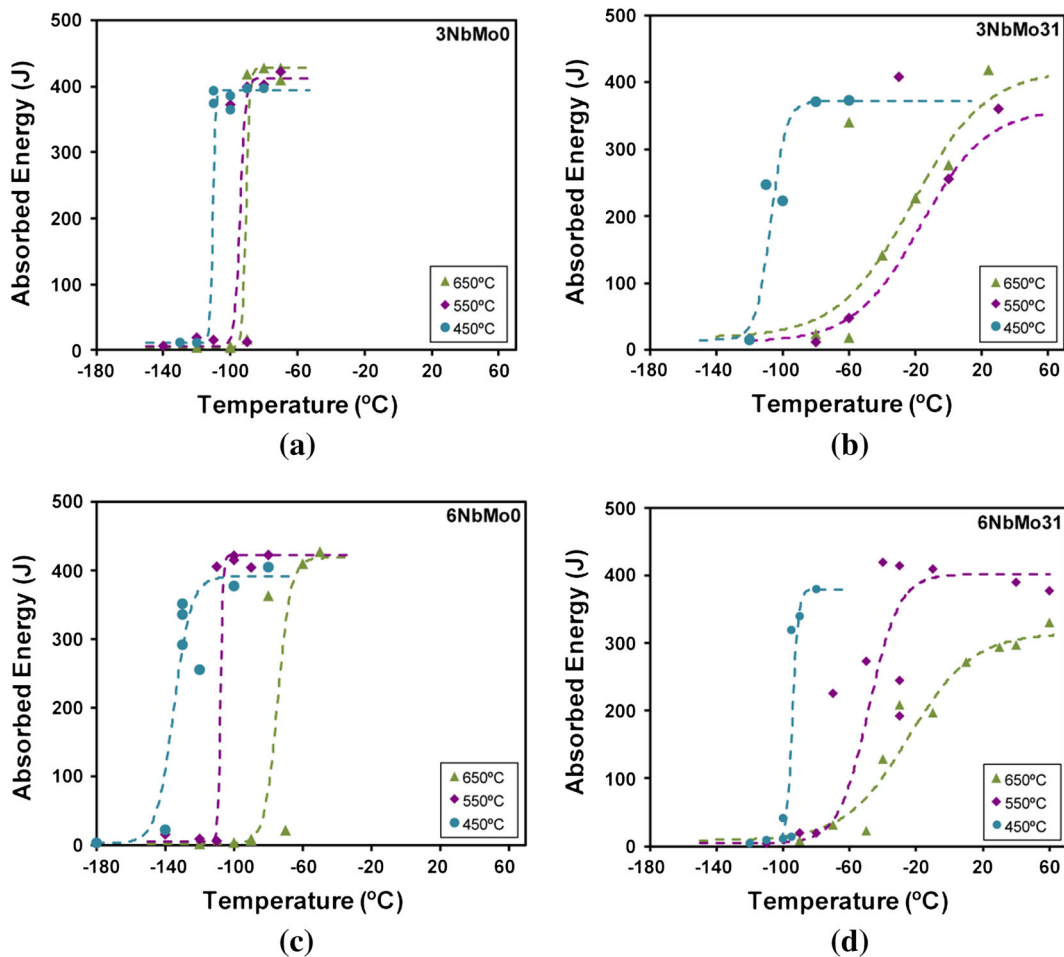


Fig. 1—Absorbed energy as a function of test temperature for all the studied steels and coiling temperatures: (a) 3NbMo0, (b) 3NbMo31, (c) 6NbMo0, and (d) 6NbMo31.

of the steel, Nb steels show lower transition temperatures when compared with Nb-Mo steels (see Figure 1; Table II). Pronounced ductile–brittle transitions are observed in Nb steels, while for Nb-Mo steels the transition ranges are wider (see Figures 1(b) and (d)). These differences are related to the presence of MA microconstituents in Nb-Mo steels, the increase of tensile properties (contribution of dislocations and precipitation) and a higher heterogeneity (formation of coarse units). These three factors will be analyzed in detail later. In Nb-Mo steels, at the coiling temperature of 723 K (450 °C), toughness properties improve noticeably with regard to higher temperatures. This improvement is mainly due to the absence of MA islands.

Detailed fractographic examination was carried out on the tested Charpy samples for the purpose of classifying and evaluating possible cleavage crack-initiation sites and microstructural features in their vicinity. Examples of different cleavage-initiation sites are shown in Figure 2. The riverline patterns indicate that these particles are the initiation points of the cleavage facets. Figures 2(a) and (b) correspond to a cleavage-initiation site due to the presence of pearlite in 3NbMo0 coiled at 923 K (650 °C) [test temperature of 153 K (–120 °C)]. Figures 2(c) and (d), steel 3NbMo31 and

test temperature of 193 K (–80 °C), show that the initiation particles have the smooth and blocky appearances typical of MA constituents. No presence of other inclusion types (oxide or nitrides) was detected in the samples. According to these observations, it can be concluded that the fracture mechanism appears to be triggered by pearlite colonies in Nb steels and MA presence in Nb-Mo steels.^[17]

IV. DISCUSSION

A. Analysis of the Effect of the Microstructure on the Toughness Properties

A detailed microstructural characterization was reported in Part I.^[3] In brief, however, a key point is that in Nb microalloyed steels, when a high coiling temperature is applied [923 K (650 °C)], the microstructure is composed of polygonal ferrite (PF) and degenerated pearlite (DP). A combination of quasipolygonal ferrite (QF) and granular ferrite (GF) is obtained when coiling temperature decreases [823 K (550 and 450 °C)]. However, the microstructures in the Nb-Mo steels (3NbMo31 and 6NbMo31) differ from the

Table II. ITT(27 J), DBTT, and US Values for Steels 3NbMo0, 3NbMo31, 6NbMo0, and 6NbMo31 and the Coiling Temperatures of 923 K, 823 K, and 723 K (650 °C, 550 °C, and 450 °C)

Steel	T_{coiling} [K (°C)]	ITT (27 J) [K (°C)]	DBTT [K (°C)]	US (J)
3NbMo0	923 (650)	179 (−94)	185 (−88)	428
	823 (550)	174 (−99)	170 (−103)	412
	723 (450)	160 (−113)	159 (−114)	394
3NbMo31	923 (650)	194 (−79)	254 (−19)	407
	823 (550)	213 (−60)	248 (−25)	352
	723 (450)	150 (−123)	183 (−90)	372
6NbMo0	923 (650)	188 (−85)	189 (−84)	422
	823 (550)	163 (−110)	169 (−104)	422
	723 (450)	124 (−149)	141 (−132)	390
6NbMo31	923 (650)	202 (−71)	243 (−30)	314
	823 (550)	198 (−75)	216 (−57)	402
	723 (450)	174 (−99)	176 (−97)	380

ones in Nb steels. At a coiling temperature of 923 K (650 °C), PF is formed accompanied by coarse MA islands. When the coiling temperature is decreased to 823 K (550 °C), the formation of QF and GF is observed with the presence of fine MA constituents. At the lowest coiling temperature of 723 K (450 °C), the microstructure is characterized by nonpolygonal phases, such as QF and GF, and no presence of MA regions retained between transformed phases is detected.

Low and high angle misorientation crystallographic unit sizes were quantified by EBSD. As mentioned in Section I, low angle unit sizes are considered effective in controlling strength properties (yield and tensile strength), acting as a barrier to dislocation movement.^[11,18] Nevertheless, high angle unit sizes provide an effective obstacle to crack propagation and control toughness properties. It is widely known that the crack deflection path is controlled by high angle boundaries and 15 deg is considered to be a threshold angle for estimating “fracture ferrite unit size”.^[11,19] Therefore, in the present study crystallographic unit sizes that consider high angle misorientation criteria have been quantified. Figure 3 shows the influence of the coiling temperature on the mean unit size for steels 3NbMo0, 3NbMo31, 6NbMo0, and 6NbMo31. As a general trend, it is evident that mean unit size decreases as the coiling temperature decreases. For example, in steel 6NbMo0, mean unit size values decrease from 4.6 to 3.1 μm , at the coiling temperature of 923 K to 723 K (650 °C and 450 °C), respectively. Furthermore, Figure 3 shows that the finest microstructures are obtained for the steels containing 0.06 pct Nb (6NbMo0 and 6NbMo31). The addition of Mo reduces the 15 deg mean unit size values in most of the cases. For example, at the coiling temperature of 723 K (450 °C), mean unit size values are 3.7 and 3.3 μm in steels 3NbMo0 and 3NbMo31, respectively. The only exception in this trend is steel 3NbMo31 and the coiling temperature of 823 K (550 °C), where its higher mean unit size is due to a bigger microstructural heterogeneity; this will be discussed later in more detail.

The effect of microstructural changes is reflected when DBTT values calculated from the Charpy curves in Figure 1 are plotted as a function of coiling temperature

(see Figure 4). As previously mentioned, the highest DBTT values are reached in Nb-Mo steels, especially for the coiling temperatures of 923 K and 823 K (650 °C and 550 °C). This trend is associated with three different microstructural features: the unit size refinement already discussed (Figure 3), the presence of MA microconstituents, and microstructural heterogeneity. These two last factors will be quantified and discussed in detail in the following subsections, but by way of general comment some facts can be highlighted following the data in Figure 4. As the coiling temperature decreases, a significant enhancement in toughness properties is achieved for all steels. The main difference between Nb and Nb-Mo steels at intermediate and high coiling temperatures is the presence of a considerable fraction of MA islands in the later which impairs toughness. In addition, the microstructural heterogeneity is also higher in Nb-Mo steels due to the presence of more bainitic structures. The differences between Nb and Nb-Mo steels are reduced at the coiling temperature of 723 K (450 °C) due to the absence of MA constituents in the latter.

Figure 5 shows tensile strength values reported in the Part I paper^[3] as a function of DBTT values for steels 3NbMo0, 3NbMo31, 6NbMo0, and 6NbMo31. Different behaviors can be detected depending on the steel composition. Different data points have been grouped to reach a better interpretation of the diagram: properties for Nb steels and properties of microstructures in Nb-Mo steels with and without MA islands. In Nb steels, the refinement of the microstructures leads to an increase in yield strength and a decrease in DBTT values. This trend is reached as coiling temperature diminishes. When Mo is added, a more complex analysis is required to evaluate the relation between tensile strength, DBTT values, and microstructural features. At intermediate and high coiling temperatures [823 K and 923 K (550 °C and 650 °C)], the addition of Mo promotes the formation of MA islands, which results in higher tensile strength but with impaired toughness properties. Nevertheless, at the lowest coiling temperature of 723 K (450 °C), a fine microstructure of QF and GF units is formed, without MA presence. This promotes an enhancement in impact properties (decreasing DBTT).

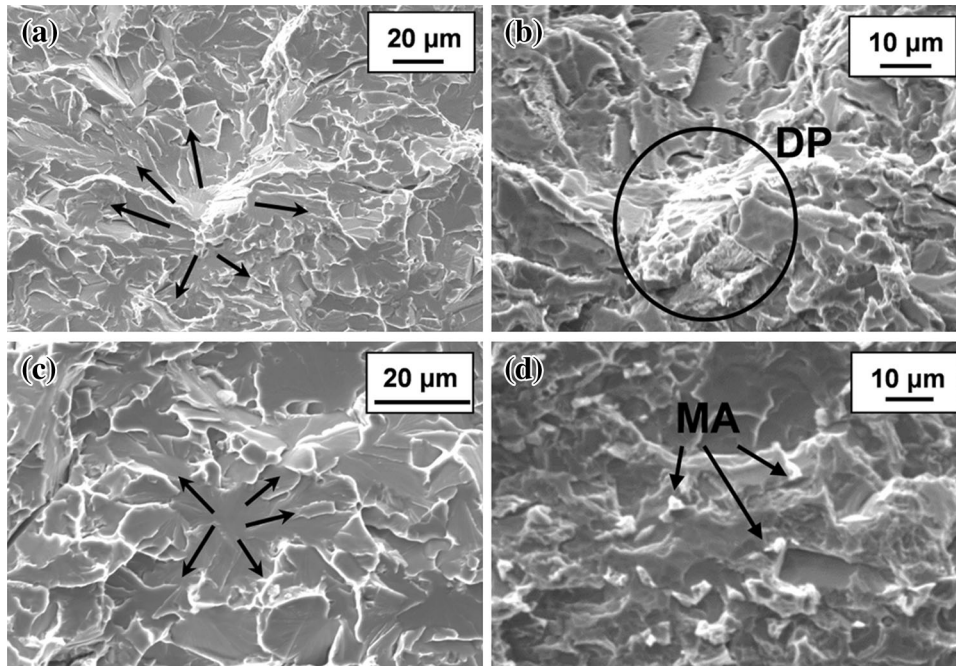


Fig. 2—Fracture images corresponding to the steel 3NbMo31 and different coiling temperatures showing the origin of the brittle fracture at secondary phases: (a) and (b) 923 K (650 °C), and (c) and (d) 823 K (550 °C). (b) and (d) show origins after etching (a) and (c), respectively. Test temperature of 193 K (−80 °C).

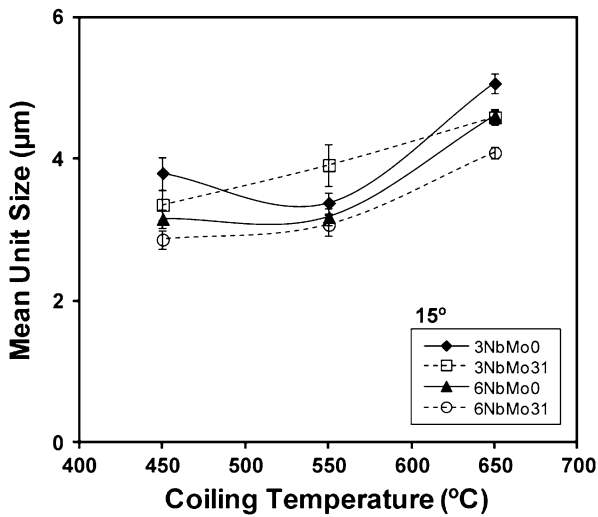


Fig. 3—Influence of coiling temperature on the average unit size for steels 3NbMo0, 3NbMo31, 6NbMo0, and 6NbMo31, using the 15 deg threshold misorientation criterion.

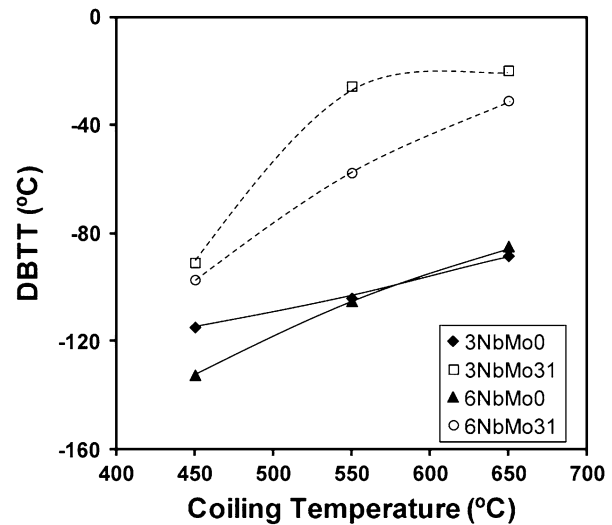


Fig. 4—DBTT values as a function of coiling temperature for steels 3NbMo0, 3NbMo31, 6NbMo0, and 6NbMo31.

1. Influence of microstructural heterogeneity

In the previous paragraphs, the importance of microstructural heterogeneity and hard phases was mentioned, but in order to incorporate these effects in the equations that predict transition temperatures a dedicated analysis and quantification is needed. Unit size distributions were measured using the EBSD scans in order to get additional information about the average unit sizes. Two examples that illustrate the microstructural differences regarding unit size distributions are shown in Figure 6, where inverse pole figures and

misorientation angle maps are plotted for steels 3NbMo0 and 3NbMo31 at the coiling temperature of 823 K (550 °C). The addition of Mo induces the presence of a more bainitic structure that is reflected in the higher fraction of low angle boundaries ($2 \text{ deg} < \theta < 15 \text{ deg}$) observed in steel 3NbMo31 (see red boundaries in Figure 6(d)). The presence of a higher fraction of nonpolygonal phases increases the heterogeneity of the microstructure^[20,21] and this is clearly observed in the higher number of coarse high angle boundary units in the microstructure.

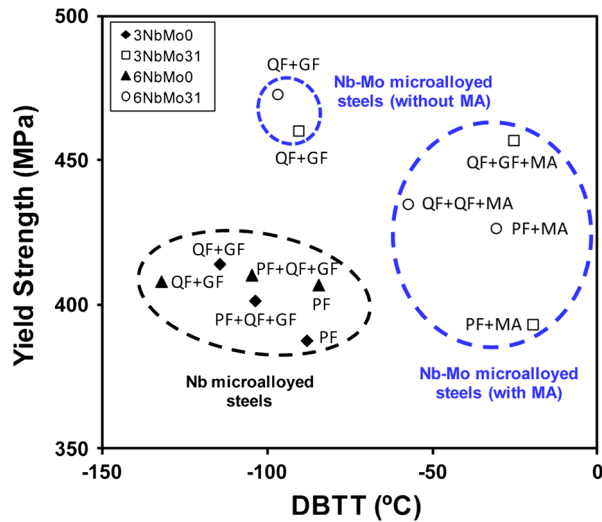


Fig. 5—Yield strength values measured in Part I paper^[3] as a function of DBTT for all the steels studied.

In Figure 7, unit size distributions considering the 15 deg high angle misorientation criterion are shown for the coiling temperature of 823 K (550 °C) and low Nb steels (3NbMo0 and 3NbMo31). A considerable influence of Mo addition on the unit size distributions is observed, obtaining a more heterogeneous distribution in steel 3NbMo31. A useful parameter to evaluate the length of the tail of a distribution is the critical grain size named as D_{c20} pct,^[22,23] which refers to the cutoff grain size at 80 pct area fraction in a grain-size distribution histogram. In Figure 7, D_{c20} pct values corresponding to both steels are indicated. D_{c20} pct values measured in the steels 3NbMo0 and 3NbMo31 are 16.7 and 37.7 μm , respectively. The increment of D_{c20} pct due to Mo addition reflects the presence of coarser grains in the resultant microstructure observed in Figure 6.

Therefore, and in order to quantify the effect of microstructural heterogeneity on ductile–brittle transition, a parameter that is able to evaluate the relevance of coarse grain fraction is required. For this purpose, the ratio between D_{c20} pct and $D_{15 \text{ deg}}$ is defined, where $D_{15 \text{ deg}}$ is the mean unit size for the 15 deg misorientation criterion. Figure 8 plots the D_{c20} pct/ $D_{15 \text{ deg}}$ ratio as a function of coiling temperature for all the steels studied. The ratio increases significantly when the coiling temperature is lowered from 923 K to 823 K (650 °C to 550 °C), and the increment is less intense for the lowest coiling temperature of 723 K (450 °C). For example, in steel 3NbMo31, the ratio increases from 3.2 to 9.2 at the coiling temperatures of 923 K and 723 K (650 °C and 450 °C), respectively. As mentioned before, the formation of a higher fraction of bainitic phases leads to an increase in heterogeneity, which is in agreement with previously published works.^[20,21] Concerning the effect of chemical composition, Figure 8 reflects a higher homogeneity for the Nb steels when compared to the Nb-Mo steels. The values corresponding to Nb steels range between 3 and 6.9, whereas D_{c20} pct/ $D_{15 \text{ deg}}$ for Nb-Mo steels varies from 3.2 to 9.6.

It is well known that the addition of Mo promotes a shift to lower transformation start temperatures in the CCT diagrams, leading to a formation of more bainitic microstructures.^[24] When PF is replaced by non-polygonal or bainitic phases, the fraction of coarse grain units increases. This fraction is lower in Nb steels and justifies the higher homogeneity of the Nb steels. For Nb-Mo steels, the microstructural heterogeneity increases as the Nb content decreases. This behavior is related to the austenite conditioning prior to transformation as the retained strain promotes a microstructural refinement and a higher fraction of PF after transformation. The higher retained strain in steel 6NbMo31 relative to steel 3NbMo31 increases the microstructural refinement, and as a consequence it limits the fraction of coarse units (*i.e.*, better homogeneity). Conversely, in steel 3NbMo31 the retained strain is lower and therefore the heterogeneity is higher. This increment in heterogeneity causes the overall coarsening of the microstructure, as reflected in the mean unit sizes in Figure 3. Therefore, from a practical point of view special attention has to be paid during austenite conditioning of Nb-Mo steels in order to maximize the retained strain in austenite *via* rolling schedule optimization^[25] and to promote fine and homogeneous microstructures after cooling.^[26,27]

2. Influence of the formation of MA islands

Besides the effect of microstructural heterogeneity, the presence of hard secondary phases affects impact toughness.^[17] The increment of DBTT for intermediate and high coiling temperatures [823 K and 923 K (550 °C and 650 °C)] in the steels containing Mo is justified by the presence of MA islands. Figures 9(a) and (b) show FEGSEM micrographs corresponding to steel 3NbMo31 at the coiling temperatures of 923 K and 823 K (650 °C and 550 °C), respectively. For the coiling temperature of 923 K (650 °C), a combination of PF and coarse MA islands is observed. When the coiling temperature is decreased, MA micro-regions retained between QF + GF are formed. It is evident that the morphology and size of MA islands differ considerably depending on the applied coiling temperature. The islands formed at the highest coiling temperature are characterized by their large size. The fractography images shown in Figure 2 confirm that the origins of the brittle fracture are associated with the MA microconstituents.

In order to evaluate the effect of the presence of MA in obtained toughness properties, MA island fraction and mean size have been quantified in the steels containing Mo. All the measurements are listed in Table III. It is observed that similar MA fractions are obtained in all the cases. However, regarding MA sizes (D_{MA}) it is evident that the decrease in the coiling temperature results in a significant refinement of the MA microconstituent. The MA size is reduced from approximately 6 to 1 μm when the coiling temperature is decreased from 923 K to 823 K (650 °C to 550 °C). Some authors suggest that the formation of MA islands results in lower ductility and toughness properties,^[28] while other works report that the presence of hard

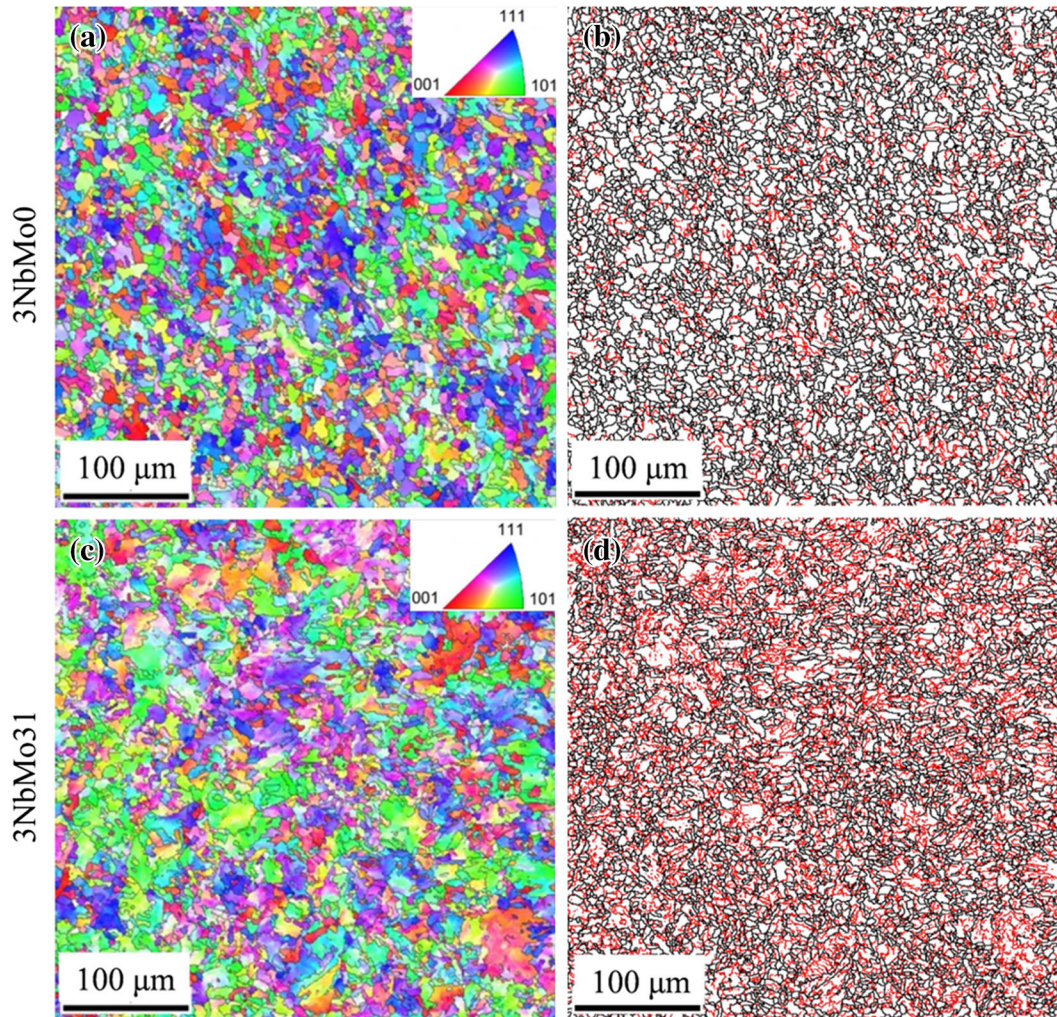


Fig. 6—Microstructural details obtained by EBSD for steels 3NbMo0 and 3NbMo31 at the coiling temperature of 823 K (550 °C): (a) and (c) Inverse Pole Figure and (b) and (d) Misorientation Angle Maps (Color figure online).

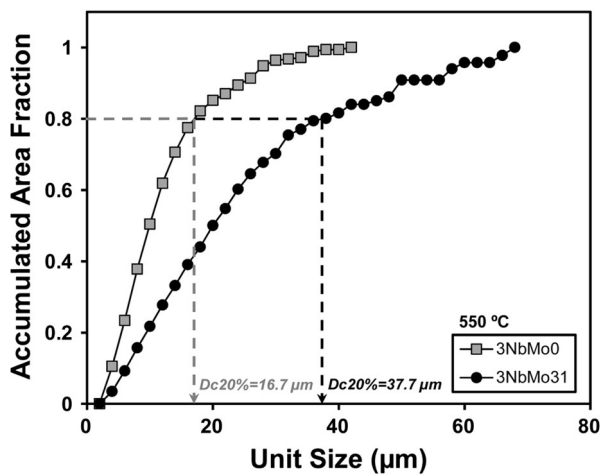


Fig. 7—Unit size distributions using 15 deg misorientation criterion plotted in terms of accumulated area for the coiling temperature of 823 K (550 °C) and steels 3NbMo0 and 3NbMo31.

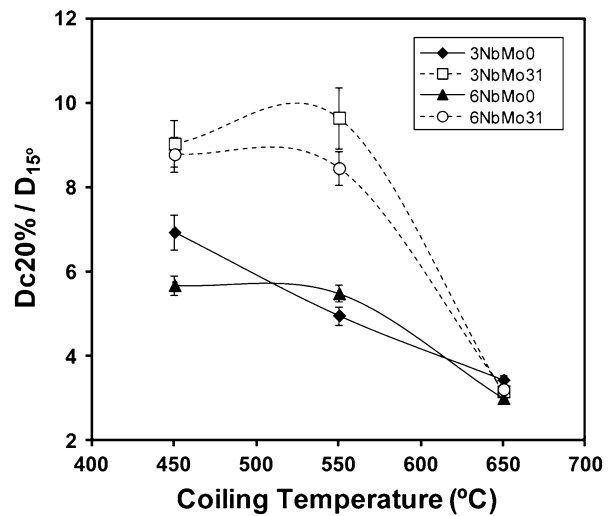


Fig. 8—Evolution of $D_{c20\%} / D_{15\text{ deg}}$ values as a function of the coiling temperature for steels 3NbMo0, 3NbMo31, 6NbMo0, and 6NbMo31.

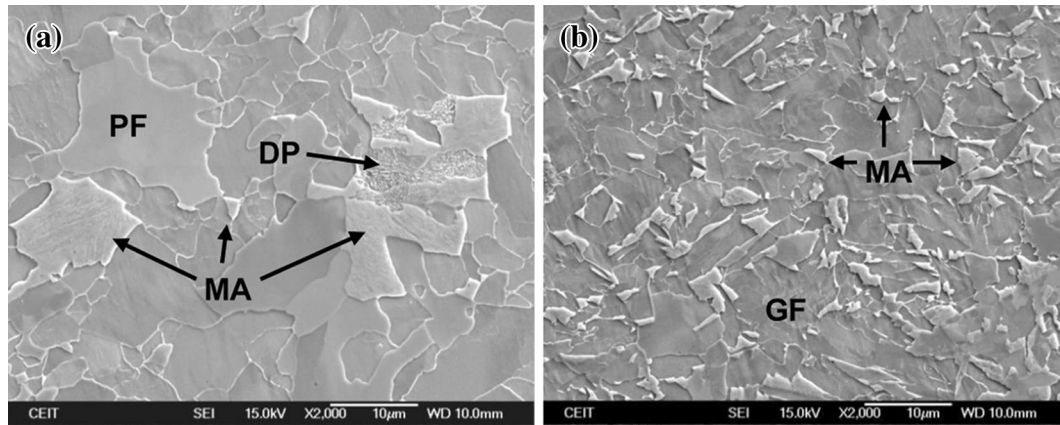


Fig. 9—General FEG-SEM micrographs of microstructures corresponding to steel 3NbMo31 at different coiling temperatures: (a) 923 K (650 °C) and (b) 823 K (550 °C).

Table III. MA Fraction and Size Values for the Steels Containing Mo (3NbMo31 and 6NbMo31) and the Coiling Temperatures of 923 K and 823 K (650 °C and 550 °C)

Steel	T_{coiling} [K (°C)]	MA Fraction (Pct)	MA Size (μm)
3NbMo31	923 (650)	11.3 ± 0.84	6.0 ± 0.04
	823 (550)	11.4 ± 0.72	1.1 ± 0.03
6NbMo31	923 (650)	9.5 ± 0.80	5.9 ± 0.02
	823 (550)	11.7 ± 0.76	1.0 ± 0.02

Table IV. Values of the Microstructural Factors Intervening in the Individual Contributions

Steel	T_{coiling} [K (°C)]	Percent Pearlite	$\Delta\sigma_y$ (MPa)	$D_{15 \text{ deg}}$ (μm)	$D_{c20 \text{ Pct}}/D_{15 \text{ deg}}$
3NbMo0	923 (650)	5.9 ± 0.7	73	5.0	3.4
	823 (550)	—	62	3.3	4.9
	723 (450)	—	80	3.7	6.9
3NbMo31	923 (650)	—	75	4.5	3.2
	823 (550)	—	102	3.9	9.6
	723 (450)	—	101	3.3	9.2
6NbMo0	923 (650)	6.5 ± 0.6	86	4.6	3.0
	823 (550)	—	89	3.1	5.4
	723 (450)	—	89	3.1	5.6
6NbMo31	923 (650)	—	82	4.0	3.2
	823 (550)	—	114	3.0	8.4
	723 (450)	—	85	2.8	8.7

phases such as MA microconstituents inside bainite could be useful for the improvement of toughness properties when fine and homogeneously distributed MA islands are attained.^[8,29,30] This is attributed to the reduction of the unit crack path due to the presence of MA regions.

B. Analysis of Microstructural Contributions in DBTT

Different relationships have been proposed in the literature to accomplish a prediction of Charpy impact transition temperatures. Some of these report different empirical equations for the temperatures required to give an impact energy value of 27 J (ITT 27 J)^[13,31] and the others are concerned about the temperature at which the sample shows a 50 pct ductile–brittle appearance (DBTT).^[32,33] A recent work on low carbon Nb-

microalloyed steels^[11] extended the existing empirical equation for the DBTT from ferrite–pearlite microstructures to high strength microstructures (bainite), where the contributions of different chemical elements and microstructural features are considered (see Eq. [2]).

$$\text{DBTT (}^\circ\text{C)} = -11\text{Mn} + 42\text{Si} + 700(N_{\text{free}})^{0.5} + 15(\text{pct Parlite})^{\frac{1}{3}} + 0.5\Delta\sigma_y - 14(D_{15 \text{ deg}})^{-0.5}. \quad [2]$$

The first two terms in Eq. [2] are related to the solid solution contribution (concentrations are expressed in wt pct). In the present steels, the substitutional solutes have a slight beneficial effect on the DBTT of approximately 15 K. Free nitrogen (N_{free}), it was calculated for

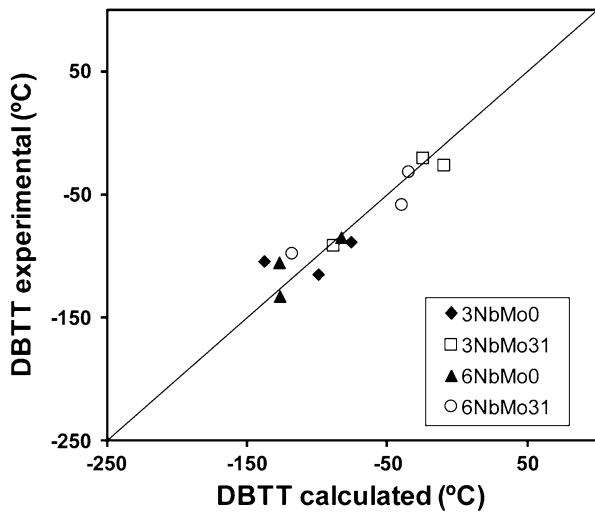


Fig. 10—Comparison between the prediction obtained by Eq. [3] and the experimental DBTT values for steels 3NbMo0, 3NbMo31, 6NbMo0, and 6NbMo31.

all the steels using Thermo-Calc software (TCFE6 database). Nitrogen is predicted to be precipitated by forming the undissolved and strain-induced niobium carbonitrides,^[34] and therefore, free nitrogen is zero at room temperature for all the steels. Percent Pearlite is the fraction of pearlite and $\Delta\sigma_y$ corresponds to the increase in yield strength due to fine precipitation and dislocations. The contributions regarding these two mechanisms are detailed in Part I.^[3] Finally, $D_{15\text{ deg}}$ accounts for the effective cleavage unit size (see Figure 3). The values for the calculations of the individual contributions are gathered in Table IV, whereas values for the MA size and fractions are reported in Table III.

In the steels under study, Eq. [2] produced an underestimation of DBTT, reflected in the prediction of higher transition temperatures than the experimentally measured ones. Therefore, in addition to the contributions considered in previously published papers, the impact of secondary hard phases and microstructural heterogeneity on the DBTT has been included. Mintz^[35] considered the detrimental influence of MA

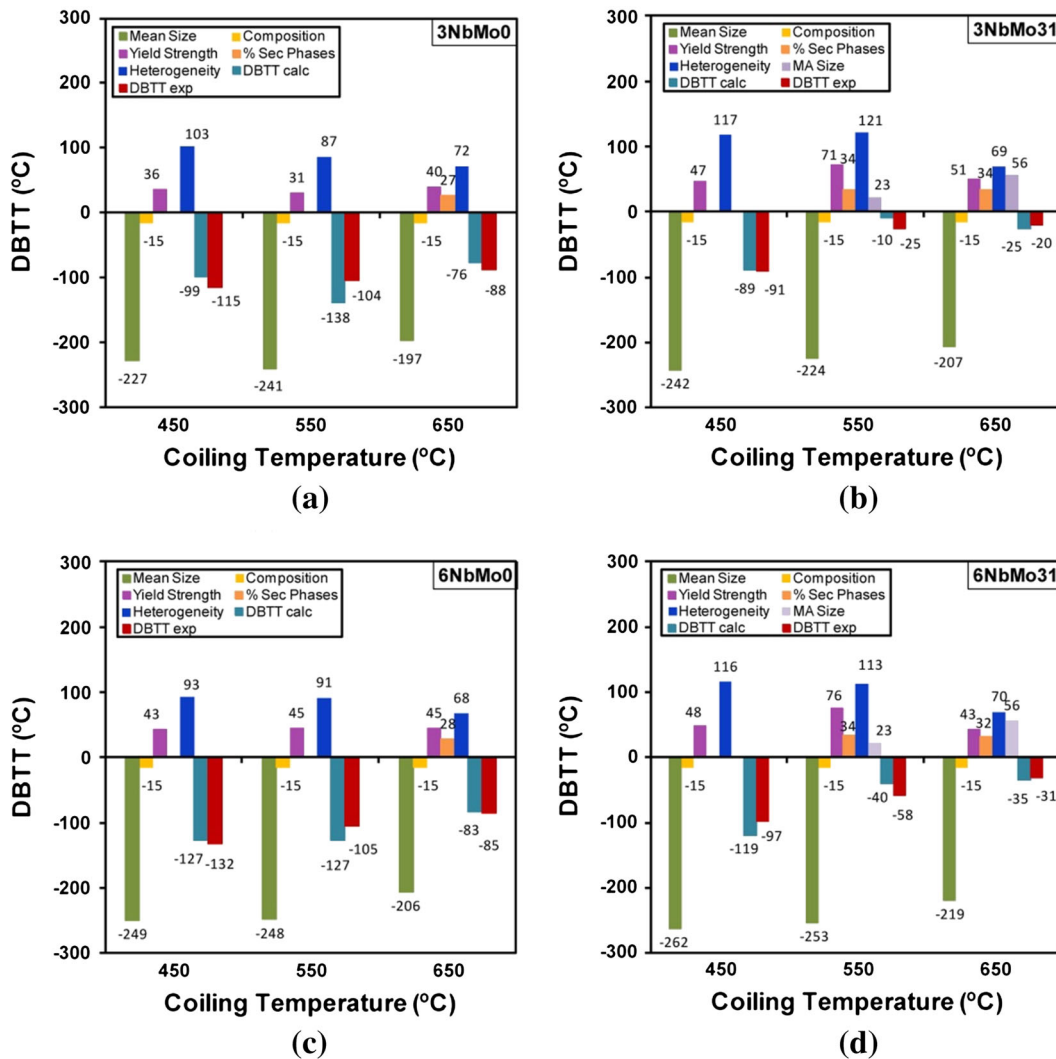


Fig. 11—Different estimated contributions to the DBTT as a function of the coiling temperature for steels (a) 3NbMo0, (b) 3NbMo31, (c) 6NbMo0, and (d) 6NbMo31 (Color figure online).

microconstituents on toughness and assumed that its effect could be similar to the effect of pearlite. Therefore, when MA is formed, the fraction of MA must be taken into account in addition to the fraction of pearlite (pct Pearlite). Regarding the effect of the size of MA islands, a relation that is similar to the carbide thickness ($t^{0.5}$) is assumed, substituting t with D_{MA} ^[13] (see values in Table III). In these steels, no grain boundary carbides were detected. Finally, the influence of heterogeneity has been included by adding an additional term with the D_{c20} pct/ $D_{15 \text{ deg}}$ factor. Both prefactors for the MA island size and the heterogeneity terms were fitted from the experimental transition temperatures and resulted in values equal to 23 and 39, respectively. The modified equation for predicting DBTT is proposed in Eq. [3]:

$$\begin{aligned} \text{DBTT } (^{\circ}\text{C}) = & -11\text{Mn} + 42\text{Si} + 700 (N_{\text{free}})^{0.5} \\ & + 15 (\text{pct Pearlite} + \text{pct MA})^{1/3} \\ & + 0.5\Delta\sigma_y - 14(D_{15 \text{ deg}})^{-0.5} \\ & + 39(D_{c20} \text{ pct}/D_{15 \text{ deg}})^{0.5} + 23 (D_{MA})^{0.5}, \end{aligned} \quad [3]$$

where pct MA and D_{MA} are the fraction and the size of the formed MA islands, respectively.

Figure 10 shows the comparisons between the prediction calculated by Eq. [3] and the experimental results (Table II) obtained from Charpy tests. A good estimation of DBTT values for entire range of coiling temperatures and steels is obtained.

Figure 11 shows the values of the individual contributions to DBTT, as well as the predicted and measured values. The contribution of the unit size and the composition are the only mechanisms that improve toughness properties. Furthermore, it is evident that the term associated with unit size is the most relevant contribution, ranging from 262 K to 197 K (-11°C to -76°C). The fine precipitates and dislocation density (included in the $\Delta\sigma_y$ term) result in an increment in the DBTT temperature. This contribution ranges between 31 K and 76 K (-242°C and -197°C). As expected, values in Figure 11 show that the new terms associated with heterogeneity and the presence of secondary phases are detrimental from the point of view of toughness. The shift in the transition temperature inferred by the heterogeneity is very important and lies between 68 K and 121 K (-205°C and -152°C). The presence of MA in the Nb-Mo steels causes an overall increment (adding pct MA and D_{MA} contributions) of about 90 K (-183°C) for the coarse MA particles [coiling temperature of 923 K (650°C)] and 57 K (-216°C) for the finer dispersion at the coiling temperature of 823 K (550°C). The interactions between grain refinement as the main mechanism lowering transition temperatures and the opposite mechanisms, such as $\Delta\sigma_y$, heterogeneity and secondary phases, which increase the transition temperature, are very complex. Therefore, the definition of an optimum balance between strength and impact toughness is only possible when suitable analysis procedures are available.

V. CONCLUSIONS

A study of the influence of coiling temperatures and alloying contents in Nb and Nb-Mo microalloyed steels on impact toughness has been performed. In addition to mechanisms such as mean crystallographic unit sizes, pearlite fraction, precipitation, and the effect of dislocation density strengthening on transition temperatures, the impact of microstructural heterogeneity and the presence of hard phases such as MA islands has been analyzed and quantified. A modified equation for predicting the DBTT that includes all the above mentioned factors has been proposed and successfully validated with the experimental results.

Low transition temperatures were achieved in Nb steels for the microstructures generated with the laboratory thermomechanical treatments. The addition of Mo increases the risk of MA formation. The impairment of the toughness properties when these hard and brittle phases are present is significant, as they become the origin for the brittle fracture. For the lowest coiling temperatures, where there is no presence of MA constituents, the transition temperatures obtained for Nb-Mo steels are very low, close to the values obtained in Nb steels.

From a practical point of view, special attention has to be paid when the alloying content increases in order to reduce microstructural heterogeneity and the presence of hard secondary phases. The optimization of the thermomechanical cycle has to seek the maximization of the retained strain in austenite during the last rolling passes in order to increase the fraction of polygonal phases after transformation. The presence of more non-polygonal bainitic areas increases microstructural heterogeneity. In addition to this, the cooling strategy and coiling process have to be controlled in order to minimize the formation of MA islands or at least reduce their size to achieve fine dispersion. The presence of coarse MA impairs transition temperatures dramatically. If these two factors are suitably controlled interesting combinations of strength and impact toughness properties are obtained in Nb and Nb-Mo microalloyed steels.

ACKNOWLEDGMENTS

The financial support of the Spanish Ministry of Economy and Competitiveness (MAT2009-09250 and MAT2012-31056) and the Basque Government (PI2011-17) is gratefully acknowledged.

REFERENCES

1. L. Bracke, N. De Wispelaere, H. Ahmed, and O.E. Gungor: *Proceedings of the International Symposium on Recent Developments in Plate Steels*, 2011, pp. 131–38.
2. D.S. Liu, B.G. Cheng, and M. Luo: *ISIJ Int.*, 2011, vol. 51, pp. 603–11.
3. N. Isasti, D. Jorge-Badiola, M.L. Taheri, and P. Uranga: *Metall. Mater. Trans. A*, DOI: [10.1007/s11661-014-2450-7](https://doi.org/10.1007/s11661-014-2450-7).

4. W. Schütz and F. Schröter: *Mater. Sci. Technol.*, 2005, vol. 21, pp. 590–96.
5. A. Ghosh, A. Ray, D. Chakrabarti, and C.L. Davis: *Mater. Sci. Eng. A*, 2013, vol. 561, pp. 126–35.
6. V.S.A. Challa, W.H. Zhou, R.D.K. Misra, R. O'Malley, and S.G. Jansto: *Mater. Sci. Eng. A*, 2014, vol. 595, pp. 143–53.
7. A. Iza-Mendia and I. Gutiérrez: *Mater. Sci. Eng. A*, 2013, vol. 561, pp. 40–51.
8. B. Wang and J. Lian: *Mater. Sci. Eng. A*, 2014, vol. 592, pp. 50–56.
9. J.M. Rodríguez-Ibabe: in *The Making, Shaping and Treating of Steels*, Flat Products Volume, AIST, 2014, pp. 113–170.
10. R. Zubialde, P. Uranga, B. López, and J.M. Rodríguez-Ibabe: in *Proc. MS&T 2013 Conf.*, Montreal, 2013, pp. 313–20.
11. I. Gutiérrez: *Mater. Sci. Eng. A*, 2013, vol. 571, pp. 57–67.
12. M.S. Bingley: *Mater. Sci. Technol.*, 2001, vol. 17, pp. 700–14.
13. B. Mintz, G. Peterson, and A. Nassar: *Ironmaking Steelmaking*, 1994, vol. 21, pp. 215–22.
14. R.L. Higginson and C.M. Sellars: *Worked Examples in Quantitative Metallography*, The Institute of Materials, Minerals and Mining, London, 2003, pp. 1–116.
15. F.S. LePera: *Metallography*, 1979, vol. 12, pp. 263–8.
16. K. Wallin: in *ECOPRESS Research Seminar on Economical and Safe Application of Modern Steels for Pressure Vessels*, Aachen, 2003.
17. P. Mohseni, J.K. Solberg, M. Karlsen, O.M. Akselsen, and E. Østby: *Metall. Mater. Trans. A*, 2014, vol. 45A, pp. 384–94.
18. M.J. Merwin, C.T. Becker, and D.R. Giansante: in *Proc. MS&T'09 Conf.*, Pittsburgh, (2009), pp. 956–68.
19. M. Díaz-Fuentes, A. Iza-Mendia, and I. Gutiérrez: *Metall. Mater. Trans. A*, 2003, vol. 34A, pp. 2505–16.
20. N. Isasti, D. Jorge-Badiola, M.L. Taheri, B. López, and P. Uranga: *Metall. Mater. Trans. A*, 2011, vol. 42A, vol. 3729–42.
21. N. Isasti, D. Jorge-Badiola, M.L. Taheri, and P. Uranga: *Metall. Mater. Trans. A*, 2013, vol. 44A, pp. 3552–63.
22. A. Fröm and R. Sandstrom: *Mater. Charact.*, 1999, vol. 41, pp. 111–22.
23. T. Hanamura, F. Yin, and K. Nagai: *ISIJ Int.*, 2004, vol. 44, pp. 610–7.
24. W.B. Lee, S.G. Hong, C.G. Park, and S.H. Park: *Metall. Mater. Trans. A*, 2002, vol. 33A, pp. 1689–98.
25. P. Uranga, A.I. Fernández, B. López, and J.M. Rodríguez-Ibabe: in *Proc. 43rd Mech. Working Steel Processing Conf.*, ISS, Warrendale, 2001, pp. 511–29.
26. M. Olasolo, P. Uranga, J.M. Rodríguez-Ibabe, and B. López: *Mater. Sci. Eng. A*, 2011, vol. 528, pp. 2559–69.
27. N. Isasti: PhD Thesis, Tecnun (University of Navarra), San Sebastian, 2013.
28. Y.M. Kim, S.Y. Shin, H. Lee, B. Hwang, S. Lee, and N.J. Kim: *Metall. Mater. Trans. A*, 2007, vol. 38A, pp. 1731–42.
29. X.Z. Zhang and J.F. Knott: *Acta Mater.*, 1999, vol. 47, pp. 3483–95.
30. S.Y. Han, S.Y. Shin, S. Lee, N.J. Kim, J.H. Bae, and K. Kim: *Metall. Mater. Trans. A*, 2010, vol. 41A, pp. 329–40.
31. J. Majta, R. Kuziak, M. Pietrzyk, and H. Krzton: *J. Mater. Proc. Technol.*, 1996, vol. 60, pp. 581–88.
32. B. Mintz, W.B. Morrison, and A. Jones: *Met. Technol.*, 1979, vol. 6, pp. 252–60.
33. F.B. Pickering and T. Gladman: *Metallurgical Developments in Carbon Steels*, Iron and Steel Inst., London, 1963, Special Report No. 81.
34. N. Isasti, D. Jorge-Badiola, M.L. Taheri, and P. Uranga: *Met. Mater. Int.*, 2014 (in press).
35. B. Mintz: *Metall. Mater. Trans. A*, 1997, vol. 28A, pp. 1997–2073.